

# The minimal channel: a fast and direct method for characterising roughness

Michael MacDonald<sup>1</sup>, Daniel Chung<sup>1</sup>, Nicholas Hutchins<sup>1</sup>, Leon Chan<sup>1</sup>, Andrew Ooi<sup>1</sup>, Ricardo García-Mayoral<sup>2</sup>

<sup>1</sup> Department of Mechanical Engineering, University of Melbourne, Victoria 3010, Australia

<sup>2</sup> Department of Engineering, University of Cambridge, CB2 1PZ, UK

E-mail: michael.macdonald@unimelb.edu.au

**Abstract.** Roughness only alters the near-wall region of turbulent flow and leaves the outer-layer unaffected, making it a prime candidate for the minimal-span channel framework which only captures the near-wall flow. Recently, Chung *et al.* (*J. Fluid Mech.*, vol. 773, 2015, pp. 418–431) showed that the minimal-span channel can accurately characterise the hydraulic behaviour of roughness. Following on from this, we aim to further optimise the minimal-span channel framework by primarily noting that the outer layer it produces is inherently incorrect, and as such modifications to this region can be made to improve performance. Firstly, a half-height channel with slip wall is shown to reproduce the near-wall behaviour seen in a standard channel, but with half the number of grid points. Next, a forcing model is introduced into the outer layer of a half-height channel. This reduces the high streamwise velocity associated with the minimal channel and allows for a larger computational time step. The streamwise length of the channel is also investigated independent of the previous improvements, and suggests the minimum length should be at least 3 times the spanwise width and also 1000 viscous-units long, whichever is longer. Finally, an investigation is conducted to see if varying the roughness Reynolds number with time is a feasible method for obtaining the full hydraulic behaviour of a rough surface, instead of running multiple simulations at fixed roughness Reynolds numbers.

## 1. Introduction

Numerical simulations of wall-bounded turbulent flows represent a challenging computational problem, as both small and large scales need to be represented. The former requires a fine grid to resolve the small viscous scales, while the latter requires a large domain to capture the large outer-layer motions. However, pioneering work by [1, 2] into minimal-flow units showed that only a small computational domain can be used to exclusively capture the turbulent near-wall cycle, independent of the large outer scales. This is achieved by simply restricting the domain of the channel to a small size, where the spanwise and streamwise lengths are prescribed in terms of viscous units. Ref. [1] showed that turbulence could be maintained in the form of the near-wall cycle of the buffer layer when the spanwise domain width was only on the order of  $100\nu/U_\tau$ ; here  $\nu$  is the kinematic viscosity and  $U_\tau = \sqrt{\tau_w/\rho}$  is the friction velocity, defined using the wall shear stress  $\tau_w$  and the fluid density  $\rho$ . This was further supported by future studies into minimal-flow units [3–5]. In particular the work of [3] showed that the minimal-span channel can also capture the logarithmic layer of turbulent flows.

An important aspect of minimal-span channels is that the near-wall flow is accurately captured up until a critical wall-normal location,  $z_c$ . Above this point, the streamwise velocity



increases compared to a full-span channel. This occurs as the narrow spanwise domain width of the minimal-span channel acts as a filter which limits the largest spanwise scale of energy-containing eddies. Note that the flow retains turbulent scales smaller than the spanwise domain width, so it is not laminar either. The critical value where the minimal-span channel departs from the full-span channel has been shown to scale with the spanwise domain width,  $z_c \approx 0.4L_y$  [5], although a constant of 0.3 is suggested in [3]. Following [3, 6], we will refer to the flow below  $z_c$  as ‘healthy’ turbulence, as it is the same as in a full-span channel. The largest captured eddy present in the domain would have a spanwise size  $\lambda_y$  that is equal to channel width,  $\lambda_y = L_y$ . In the logarithmic region of the flow, the streamwise length of quasi-streamwise vortices scale as roughly 2–3 times the spanwise width,  $\lambda_x \approx 2\text{--}3\lambda_y$  [3, 7].

In the context of roughness, the central question is how to relate the geometry of a rough surface to its hydraulic behaviour; namely, what value the (Hama) roughness function,  $\Delta U^+$ , takes [8]. This quantity reflects the flow retardation, or velocity shift, that the roughness has on the flow when compared to a smooth wall, for matched friction Reynolds numbers,  $Re_\tau = U_\tau h/\nu$  (here  $h$  is the half-channel height, boundary layer thickness, or pipe radius). For a given surface,  $\Delta U^+$  can be obtained from various models and approximations, or directly from full-scale experiments and numerical simulations. The former are of varying accuracy and depend on the model selected and the rough surface in question, while the latter can be prohibitively expensive. In particular, full scale numerical simulations suffer from the drawbacks mentioned above, in that both small- and large-scale motions need to be captured. However, roughness is thought to primarily alter only the near-wall flow, in a region called the roughness sublayer which extends  $3\text{--}5k$  from the wall, where  $k$  is some characteristic height of the roughness [9]. Outside the roughness sublayer, in the outer layer, the flow is only changed insofar as it depends on the friction velocity  $U_\tau$ . This is the basis of Townsend’s outer-layer similarity hypothesis [10] which has received significant attention and has been supported by several rough-wall studies [9, 11, 12] and also numerical simulations with modified boundary conditions [13–15]. If we assume Townsend’s hypothesis holds, then it follows that the roughness only alters the near-wall region of the flow which therefore makes it a prime candidate for use in the minimal-flow framework.

Recently, we have applied the idea of minimal-span channels to the roughness problem [5]. It was shown that the roughness function could be accurately computed from minimal-span channels, when compared with full-span channels. However, the use of minimal-span channels has some drawbacks; namely the flow is ‘bursty’, resulting in large fluctuations in the flow statistics over time, which requires a long averaging time to obtain statistically stationary data. Another issue is that the streamwise velocity is extremely large in the altered outer layer above  $z_c$ , which places a restriction on the time step due to the Courant-Friedrichs-Lewy (*CFL*) condition.

In this paper, we aim to improve the minimal-span channel method for roughness. This is achieved by noting that the outer layer in minimal-flow units is meaningless as it does not represent a true turbulent flow, so alterations to this region are made while ensuring the near-wall behaviour remains unchanged. To this end, a series of optimisations to the minimal channel are performed. Firstly, only half of the channel is simulated, with a slip wall placed at the channel centreline. Second, a forcing model is applied to the outer layer of the half-height channel, to reduce the centreline velocity and improve the computational time step. Finally, an investigation of the streamwise domain length is performed, independent of the previous improvements. While the flow will still be bursty, which is an intrinsic aspect of minimal flow units [16, 17], these improvements reduce the impact that it has as the long time-scale burstiness can be simulated faster. Finally, an investigation independent of the previous improvements is conducted in which the bulk velocity (and hence roughness Reynolds number) is varied with time, to see if the full hydraulic behaviour of the rough surface can be obtained. This is of interest as currently multiple (steady) simulations are needed to obtain the  $\Delta U^+$  vs  $k^+$  curve.

## 2. Numerical Method

We conduct Direct Numerical Simulations (DNS) using the same finite difference code as in [5], which uses a fully conservative fourth-order staggered-grid scheme. Time integration is performed using the third-order low-storage Runge–Kutta scheme of [18], and the fractional-step method of [19] is used. The Navier–Stokes equations are

$$\nabla \cdot \mathbf{u} = 0, \quad \frac{\partial \mathbf{u}}{\partial t} + \nabla \cdot (\mathbf{u}\mathbf{u}) = -\frac{1}{\rho} \nabla p + \nabla \cdot (\nu \nabla \mathbf{u}) + \mathbf{F} + \mathbf{G} + \mathbf{K}, \quad (1)$$

where  $\mathbf{u} = (u, v, w)$  is the velocity in the streamwise ( $x$ ), spanwise ( $y$ ) and wall-normal ( $z$ ) directions,  $t$  is time, and  $p$  is pressure.  $\mathbf{G} = G_x(t)\mathbf{i}$  is the spatially invariant, time-varying streamwise forcing term which drives the flow at constant mass flux. The flow is solved in a moving reference frame so that the mass flux is zero at all times, although all equations in this paper are given in the stationary reference frame. Solving in a moving reference frame permits a larger computational time step [20], as well as reducing high-wavenumber convective disturbances produced by finite difference schemes [21].  $\mathbf{F} = -\alpha F(z, k)u|\mathbf{i}$  is a roughness model based on the work of [22] which applies a forcing in the streamwise direction which opposes the flow. The roughness factor  $\alpha = 1/(40k)$  is kept constant for all simulations, with the roughness height  $k = h/40$ . The function  $F(z, k)$  is a simple step function which applies the roughness forcing close to the top and bottom no-slip channel walls at  $z = 0$  and  $z = 2h$ ,

$$F(z, k) = \begin{cases} 1, & \text{if } z < k \text{ or } 2h - k < z. \\ 0, & \text{otherwise.} \end{cases} \quad (2)$$

This roughness model removes any spanwise or streamwise roughness length scales from the problem and allows for simpler computations as the same smooth-wall grid can be used. This is a similar approach to [23], although there the author used an  $\mathbf{F} \propto u\mathbf{i}$  scaling. The final term in (1),  $\mathbf{K}$ , is a forcing function which damps the velocity in the outer layer of the minimal channel. It has the form

$$K_i = -\lambda \Gamma(z, z_d) \left( u_i(x, y, z, t) - \langle u_i \rangle(z_d, t) \right) \left| u_i(x, y, z, t) - \langle u_i \rangle(z_d, t) \right|, \quad (3)$$

where angled brackets denote the spatial average of the instantaneous velocity over a wall-parallel plane. The factor  $\lambda$  has units of inverse time and in this study has a value of  $\lambda h/U_\tau \approx 1$ . The parameter  $\Gamma(z, z_d)$  is similar to the function  $F(z, k)$  of the roughness forcing model in that it prescribes where the damping is applied, namely in the outer layer of the channel,

$$\Gamma(z, z_d) = \begin{cases} 1, & \text{if } z > z_d \text{ and } z < 2h - z_d. \\ 0, & \text{otherwise.} \end{cases} \quad (4)$$

The value of  $z_d$  should be greater than the critical wall-normal location,  $z_c$ , of the minimal-span channel, so that the forcing does not contaminate the healthy turbulence of the near-wall flow. Several different values of  $z_d$  are tested and will be presented in the following section. In (3), the term  $\langle u_i \rangle(z_d, t)$  is the wall-parallel spatially averaged velocity at  $z_d$ . This is present to reduce the magnitude of the streamwise velocity; the minimal channel has a very high streamwise velocity which presents a time step restriction from the  $CFL$  number. The forcing is in this form so that the velocity is forced to remain at the same level as at  $z = z_d$ . This outer-layer damping is similar to the masks employed in [6], which damp fluctuations in the outer-layer region of minimal channels. The current forcing model is fairly crude in that it simply sets the streamwise velocity to be approximately that at  $z = z_d$ , however it will be shown to work reasonably well for the

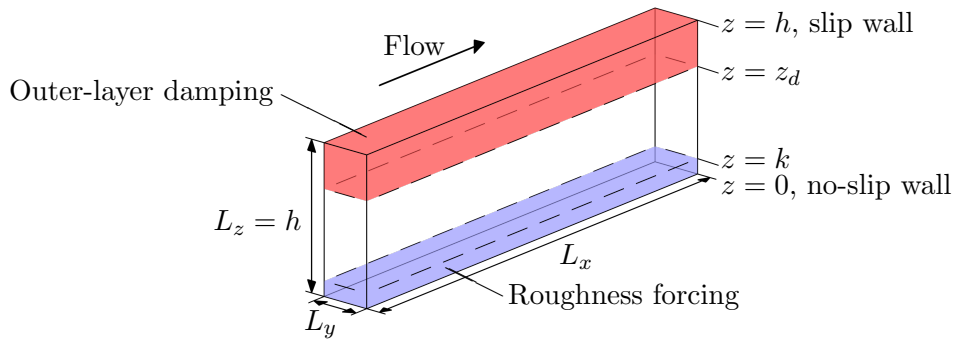


Figure 1: Half-height minimal-span channel, showing the roughness forcing zone (2) and the outer-layer damping zone (3). No-slip wall at  $z = 0$  and slip wall at  $z = h$ .

purpose of obtaining  $\Delta U^+$ . Note that the average velocity in the spanwise and wall-normal directions is zero, so that the forcing in these directions can simply be  $K_i = -\lambda\Gamma(z, z_d)u_i|u_i|$ , for  $i = 2, 3$ . Figure 1 shows the two forcing regions that are employed in the current study.

The streamwise and spanwise grid is evenly spaced, while the wall-normal grid is stretched with a cosine mapping. Periodic boundary conditions are applied in the spanwise and streamwise directions. In the case of standard-height channels, no-slip walls are located at  $z = 0$  and  $z = 2h$ . For clarity, the word ‘full’ will be used to refer to the span (full span), while the case with two no-slip walls will be referred to as ‘standard’ height. For half-height (open) channels, a no-slip wall is still positioned at  $z = 0$ , however now the top domain surface is a slip wall with  $\partial u/\partial z = \partial v/\partial z = 0$ , positioned at  $z = h$ . This slip wall maintains the impermeability constraint,  $w = 0$ . The spanwise width,  $L_y$ , of the minimal-span channel follows the guidelines of [5]. Simulation parameters are given in table 1. For each entry, both a smooth wall and modelled rough wall are simulated with the stated parameters.

### 2.1. Temporal sweep

The equivalent sandgrain roughness,  $k_s^+$ , is a single dynamic parameter that is used to describe the hydraulic behaviour of roughness. It is defined so that the roughness function collapses for all data in the fully rough regime, when the friction factor no longer depends on the bulk-velocity Reynolds number [24]. However, each rough surface will have a unique behaviour in the transitionally rough regime. It is an expensive process to determine the full hydraulic behaviour, as a range of simulations need to be conducted for the different roughness Reynolds numbers, each requiring a different body-fitted grid. Moreover, for constant mass flux simulations as in this study, the mass flux is altered until the friction Reynolds number is close to the desired value. The log layer of the flow is not easily identifiable for low Reynolds number simulations, so the roughness function is calculated assuming the smooth- and rough-wall flows have matched  $Re_\tau$ . This means that differences in  $Re_\tau$  introduce a level of uncertainty into the estimate of  $\Delta U^+$ . It is desirable to conduct a simulation in which only a single grid is used, and the bulk velocity is changed over time. This is a similar approach to how experimental studies are performed, and will allow a sweep through a range of roughness Reynolds numbers. In order to obtain statistics at a desired friction Reynolds number, the flow is averaged over a small window in which the instantaneous friction Reynolds number is close to the desired one. Within this window, the flow is assumed to be quasi steady. An important consideration which will be investigated here is whether acceleration effects become significant and distort the estimation of  $\Delta U^+$ , that is, how quickly can the bulk velocity be varied.

The sweep will start with the highest friction number to be tested,  $Re_{\tau, start}$  and will then be decelerated via an adverse pressure gradient. This results in the  $CFL$  restriction gradually reducing as the simulation progresses and also ensures an adequate grid resolution at the start

Table 1: Description of the simulations performed. All simulations done as both smooth and rough walls. Entries:  $Re_\tau$ , nominal friction Reynolds numbers;  $L$ , domain length;  $N$ , number of grid points;  $\Delta$ , grid-spacing in viscous units, subscript  $w$  and  $h$  refers to the wall-normal grid spacing at the wall and channel centre;  $z_d^+$ , location where the outer-layer damping begins (3).  $L_z/h = 2$  denotes standard-height (two no-slip walls),  $L_z/h = 1$  denotes half-height channel (one no-slip wall and one slip wall).  $\Delta t_S^+$  and  $\Delta t_R^+$  is the smooth- and rough-wall time step. Roughness height fixed at  $k = h/40$  so  $k^+ \approx 15$  at  $Re_\tau = 590$ , and  $k^+ \approx 50$  at  $Re_\tau = 2000$ .

$Re_\tau$	$\frac{L_x}{h}$	$L_x^+$	$L_y^+$	$\frac{L_z}{h}$	$N_x$	$N_y$	$N_z$	$\Delta x^+$	$\Delta y^+$	$\Delta z_w^+$	$\Delta z_h^+$	$z_d^+$	$\Delta t_S^+/\Delta t_R^+$
$S_1$ : Full-span channel													
590	$2\pi$	3707	1854	2	384	384	256	9.7	4.8	0.04	7.2	-	0.26/0.29
590	$2\pi$	3707	1854	1	384	384	128	9.7	4.8	0.04	7.2	-	0.29/0.32
$S_2$ : Minimal-span channel													
590	$2\pi$	3707	118	2	384	24	256	9.7	4.9	0.04	7.2	-	0.35/0.40
590	$2\pi$	3707	118	1	384	24	128	9.7	4.9	0.04	7.2	-	0.36/0.41
590	$2\pi$	3707	236	2	384	48	256	9.7	4.9	0.04	7.2	-	0.37/0.39
2000	$0.59\pi$	3707	300	1	384	60	384	9.7	5.0	0.02	8.2	-	0.24/0.31
$S_{3a}$ : Minimal-span, half-height channel with outer-layer damping													
590	$2\pi$	3707	118	1	384	24	128	9.7	4.9	0.04	7.2	100	0.48/0.59
590	$2\pi$	3707	118	1	384	24	128	9.7	4.9	0.04	7.2	150	0.46/0.54
590	$2\pi$	3707	118	1	384	24	128	9.7	4.9	0.04	7.2	200	0.44/0.51
590	$2\pi$	3707	118	1	384	24	128	9.7	4.9	0.04	7.2	300	0.41/0.47
$S_{3b}$ : Minimal-span, half-height channel with outer-layer damping (wider span)													
590	$2\pi$	3707	236	1	384	48	128	9.7	4.9	0.04	7.2	200	0.43/0.48
590	$2\pi$	3707	236	1	384	48	128	9.7	4.9	0.04	7.2	250	0.43/0.47
590	$2\pi$	3707	236	1	384	48	128	9.7	4.9	0.04	7.2	300	0.42/0.46
$S_{3c}$ : Minimal-span, half-height channel with outer-layer damping (increased $Re_\tau$ )													
2000	$0.59\pi$	3707	300	1	384	60	384	9.7	5.0	0.02	8.2	300	0.25/0.37
2000	$0.59\pi$	3707	300	1	384	60	384	9.7	5.0	0.02	8.2	400	0.24/0.35
$S_{4a}$ : Minimal-span, standard-height channel, varying streamwise length													
590	$0.1\pi$	185	118	2	24	24	256	7.7	4.9	0.04	7.2	-	0.28/0.32
590	$0.16\pi$	297	118	2	48	24	256	6.2	4.9	0.04	7.2	-	0.24/0.27
590	$\pi/4$	463	118	2	48	24	256	9.7	4.9	0.04	7.2	-	0.36/0.42
590	$\pi/2$	927	118	2	96	24	256	9.7	4.9	0.04	7.2	-	0.36/0.42
590	$\pi$	1854	118	2	192	24	256	9.7	4.9	0.04	7.2	-	0.36/0.41
$S_{4b}$ : Minimal-span, standard-height channel, varying streamwise length (wider span)													
590	$0.1\pi$	185	354	2	24	72	256	7.7	4.9	0.04	7.2	-	0.37/0.45
590	$0.16\pi$	297	354	2	48	72	256	6.2	4.9	0.04	7.2	-	0.31/0.40
590	$\pi/4$	463	354	2	48	72	256	9.7	4.9	0.04	7.2	-	0.46/0.52
590	$\pi/2$	927	354	2	96	72	256	9.7	4.9	0.04	7.2	-	0.43/0.46
590	$\pi$	1854	354	2	192	72	256	9.7	4.9	0.04	7.2	-	0.38/0.40
$S_5$ : Temporal sweep (at initial conditions)													
590	$2\pi$	3707	354	2	384	80	256	9.6	4.4	0.04	7.2	-	0.38/0.43

of the simulation. This means that at the final friction Reynolds number,  $Re_{\tau,end} < Re_{\tau,start}$ , the grid resolution would be finer than necessary, which for the current simulations would have 4–5 times more cells than if a conventional steady simulation were conducted.

Models for how to vary the bulk velocity over time,  $U_b(t)$ , could be made to ensure that there occurs a certain number of turnover times of the largest captured eddy in the minimal-span

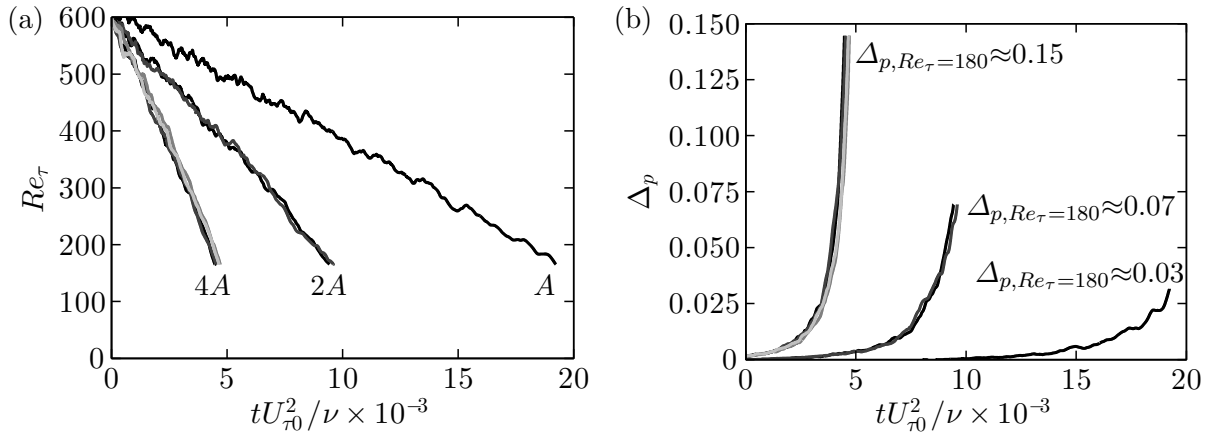


Figure 2: (a) Instantaneous Reynolds number and (b) pressure gradient parameter (6) of the smooth-wall temporal sweep, against viscous time. The cases with faster sweeps have multiple runs (shown by grey lines) and are ensemble averaged.  $A$  is the linear rate of change of  $U_b$  (5).

channel. This would require information on the characteristic time scale of the eddies, which would change with  $Re_\tau$ . However, as a preliminary study into the feasibility of this approach, we will vary it linearly with time,

$$dU_b/dt = A = (U_{b,end} - U_{b,start})/\Delta T, \quad (5)$$

where  $U_{b,end}$  is the desired end point of the simulation (the bulk velocity corresponding to  $Re_\tau = 180$ ), and  $\Delta T$  is a time scale which should be sufficiently long enough that acceleration effects are not significant to the flow. The initial bulk velocity,  $U_{b,start}$ , is set corresponding to a friction Reynolds number of  $Re_{\tau,start} = 590$  and different values of  $A$  are tested. An initial value of  $A$  is selected such that over the course of the sweep  $tU_{\tau 0}/h = 30$ , with subsequent runs using  $2A$  and  $4A$ . In these cases of a higher rate of change of  $U_b$ , multiple sweeps are run from different initial conditions with the results ensemble averaged, to ensure that statistics are obtained over the same amount of simulation time. For example, the case where the gradient is quadrupled, four sweeps are conducted with four different initial conditions. This is visualised in figure 2(a), which shows the change in the friction Reynolds number as a function of time. An important consideration with this technique is that the friction velocity and hence the normalised spanwise domain width  $L_y^+$  will vary with time. The domain width must remain larger than 100 viscous units at all times to ensure the turbulent flow is sustained, which may necessitate multiple stages in the sweep if  $L_y^+$  becomes too small. Each stage in the sweep should be set up such that  $L_y^+ \gtrsim 100$ .

A non-dimensional measure of the flow acceleration is the pressure gradient parameter,

$$\Delta_p = \frac{\nu}{\rho U_\tau^3} \frac{dp}{dx}. \quad (6)$$

Various experimental studies of decelerating boundary layers show that mild decelerations of  $\Delta_p < 0.01$  have small ( $< 3\%$ ) errors in calculating  $U_\tau$  from methods based on assuming zero pressure gradients [25, 26]. While we are interested in channel flow as opposed to boundary layers, this value should still be useful in providing an indication as to whether acceleration effects will be significant. Ref. [27], meanwhile, compared a step acceleration with a slow ramp up in which the bulk velocity was linearly varied in a channel such that  $-\Delta_p \approx 0.73$  (favourable pressure gradient). Acceleration effects were still seen in this slow ramp up. Note

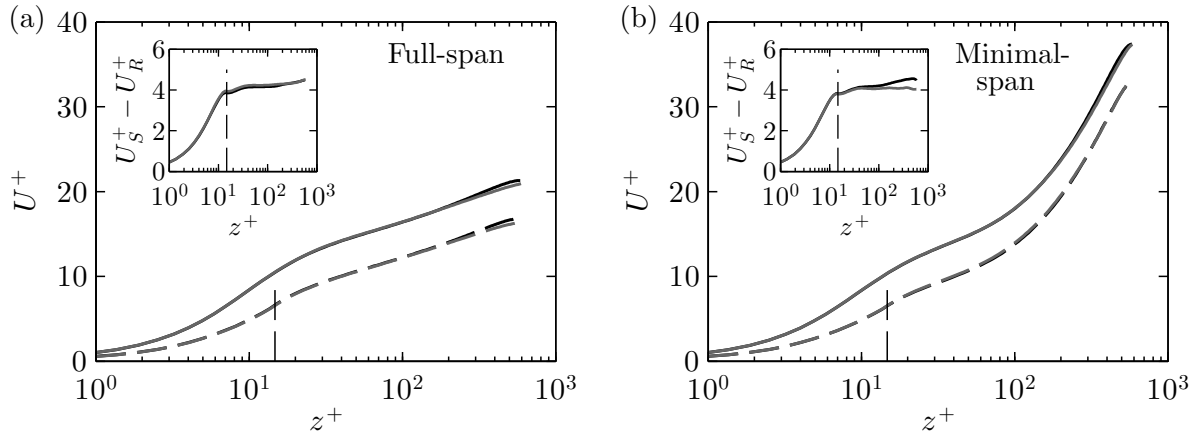


Figure 3: Mean streamwise velocity against wall-normal position for (a) full-span channel (set  $S_1$ ) and (b) minimal-span channel (set  $S_2$ ). Line styles are: black, standard-height channel; grey, half-height channel; solid, smooth wall; dashed, rough-wall model. Vertical dashed line shows roughness crest,  $k = h/40$ . Inset shows difference in smooth- and rough-wall velocity,  $U_S^+ - U_R^+$ .

that for steady channel flow, the pressure gradient parameter is  $\Delta_p = -1/Re_\tau < 0$ , which for the current simulations at  $Re_\tau = 590$  takes a value of  $-0.0017$ . In the current study, three different sweep rates are studied. As shown in figure 2(b), the linear variation in  $U_b$  results in the pressure gradient parameter being maximum at the end of the simulation, when  $Re_\tau \approx 180$ . The different sweeps will therefore be referred to by their maximum pressure gradient parameter, which are  $\Delta_{p, Re_\tau=180} \approx (0.03, 0.07, 0.15)$ . These values place the sweeps considered in this study into the range between negligible ( $\Delta_p < 0.01$ ) and noticeable ( $-\Delta_p > 0.73$ ) pressure gradient effects, and are much larger than the steady value ( $-\Delta_p = 0.0017$ ).

### 3. Results

#### 3.1. Half-height channel (sets $S_1$ and $S_2$ )

The effect of using a half-height (open) channel is investigated first. This channel has a slip wall positioned at the channel centreline, so only half of the channel needs to be simulated. This reduces the size of the grid by a half when compared to a conventional standard-height channel with two no-slip walls. The simulations are detailed in table 1 as sets  $S_1$  and  $S_2$ . Here, the streamwise length is fixed at  $L_x^+ \approx 3700$  and there is no outer-layer damping,  $K_i = 0$ .

Figure 3 shows the effect of the half-height channel in terms of the mean velocity profile, when compared to the standard-height channel. This is done for both smooth and rough walls, as well as full-span and minimal-span channels. For clarity, the full-span and minimal-span channels are shown in different figures, however the near-wall behaviour is identical up until  $z_c = 0.4L_y \Rightarrow z_c^+ \approx 50$ , as observed in [5]. Both sets of figures show that the use of the half-height channel with slip wall has a negligible effect on the flow. The main difference is seen in the wake region, where the half-height channel restricts the outer-layer structures, resulting in a slight decrease in the mean velocity. Crucially, this difference is the same for both smooth and rough walls, meaning that the difference between them,  $U_S^+ - U_R^+$ , is the same. Moreover, the change in the half-height channel occurs above the critical wall-normal location, where the minimal-span flow is already altered compared to the full-span flow. The root-mean-squared velocity fluctuations (not shown) also show good agreement between half- and standard-height channels in the near-wall region, in agreement with previous open channels [28–30]. There is some variation between the two in the outer region although this is to be expected.

Essentially, the near-wall flow is preserved, despite the imposition of an outer-layer boundary

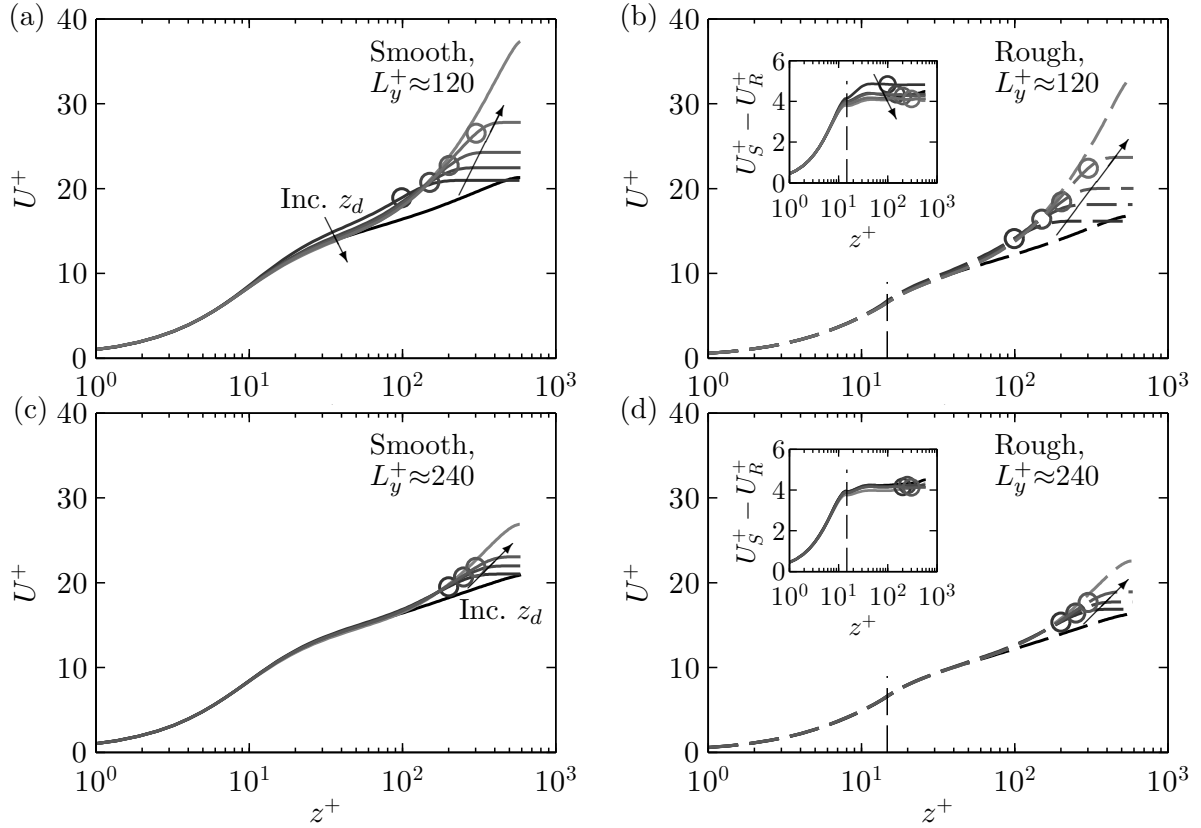


Figure 4: Streamwise velocity profile for outer-layer damping for (a,c) smooth- and (b,d) rough-wall half-height channels. Spanwise domain width is (a,b)  $L_y^+ \approx 120$  (set  $S_{3a}$ ) and (c,d)  $L_y^+ \approx 240$  (set  $S_{3b}$ ). Line styles are: black, full-span channel; grey, minimal-span channel with outer-layer damping (3) for varying damping heights of (a,b)  $z_d^+ = [100, 150, 200, 300]$  and (c,d)  $z_d^+ = [200, 250, 300]$ , shown by circles; light-grey, minimal-span with no damping. Vertical dashed line indicates the roughness height  $k = h/40$ . Inset of (b,d) shows the difference in smooth- and rough-wall velocity. Arrows indicates trend of increasing  $z_d$ .

condition. This echoes the work of [6], who showed that the near-wall cycle is preserved despite damping of outer-layer fluctuations. The half-height channel is effectively a less restrictive boundary condition than this damping, as the flow retains velocity fluctuations in the outer-layer. Importantly, it shows that only half the domain needs to be simulated without significant near-wall detriment.

### 3.2. Outer-layer damping (sets $S_{3a}$ , $S_{3b}$ , and $S_{3c}$ )

The outer-layer flow is now damped through use of the  $K_i$  forcing term (3) in a half-height channel. This is done to reduce the large centreline velocity (figure 3b) of the minimal-span channel, which places a restriction on the time step due to the  $CFL$  number. The streamwise domain length is fixed at  $L_x^+ \approx 3700$ , and other relevant parameters are detailed in table 1 under set  $S_3$ . The height where the damping begins,  $z_d$ , is investigated with several different positions in channels of two different spanwise widths;  $L_y^+ \approx 120$  (set  $S_{3a}$ ) and  $L_y^+ \approx 240$  (set  $S_{3b}$ ). These minimal channels will have a healthy turbulence region up to  $z_c^+ \approx 47$  and  $z_c^+ \approx 94$ , respectively.

Figure 4 shows the mean streamwise velocity profile for smooth- and rough-wall minimal-span channels, for both of the spanwise widths. The smallest spanwise width,  $L_y^+ \approx 120$  (figure 4a,b)



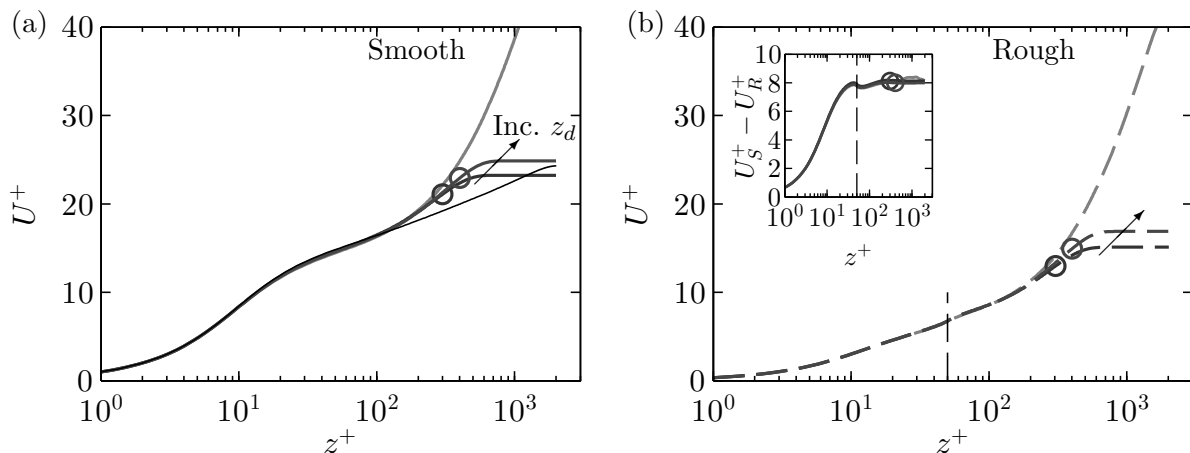


Figure 5: Streamwise velocity profile for (a) smooth- and (b) rough-wall half-height channels at  $Re_\tau = 2000$  (set  $S_{3c}$ ). Line styles are same as figure 4, however full-span smooth-wall channel data taken from [31] and damping heights are  $z_d^+ = [200, 300]$ , shown by circles.

has four different positions for  $z_d$  examined, with values of  $z_d^+ = (100, 150, 200, 250)$ . In all cases, the damping tries to restricts the streamwise velocity above  $z > z_d$  to the value of  $U(z = z_d)$ . It is clear in the smooth-wall flow (figure 4a) that the two smallest values of  $z_d^+ = 100$  and  $150$  are too close to the wall, resulting in an increase in the streamwise velocity below  $z_d$ . In particular,  $z_d^+ = 100$  results in an obvious overestimation of  $\Delta U^+$ , as seen in the inset of figure 4(b). A value of  $z_d^+ = 150$  has a similar, although not as strong of an effect. This is clearly not desirable and suggests that a value of  $z_d^+ \geq 200$  is recommended for this spanwise width.

To investigate how the location of  $z_d$  is related to  $z_c$  will require cases with a larger spanwise domain width, as  $z_c \approx 0.4L_y$ . This is done in figure 4(c,d), where the spanwise width is now  $L_y^+ \approx 240$ . Here, three different positions for  $z_d$  are analysed, with values of  $z_d^+ = (200, 250, 300)$ . There is little difference in the near-wall profiles of the three different  $z_d$  positions. This suggests that, even though  $z_c$  has doubled, we still require the damping to begin at least 200 viscous-units away from the wall. Having the outer-layer damping begin closer to the wall (i.e. reducing  $z_d$ ) seems to lead to an increase in viscous stress in the log-layer and even buffer layer (figure 4a), resulting in an overestimation of the mean streamwise velocity.

Next, the friction Reynolds number is increased to  $Re_\tau = 2000$  (set  $S_{3c}$ ). Since the roughness height is fixed as a ratio of the channel half-height,  $k = h/40$ , then the roughness Reynolds number increases to  $k^+ = 50$ . The spanwise width also needs to be increased to submerge the roughness sublayer in healthy turbulence [5], here it takes a value of  $L_y^+ = 300$  so that the critical wall-normal location is  $z_c^+ \approx 120 = 2.4k$ . Figure 5 shows the mean velocity profile for these higher  $Re_\tau$  simulations in which  $z_d^+ = (200, 300)$ . Only smooth-wall full-span channel data is available from [31] to compare with the minimal-span channel, and good agreement is seen up until  $z^+ \approx 120$  (figure 5a). Here, both positions of  $z_d$  produce velocity profiles which compare well with the minimal-span channel with no outer-layer damping.

Recall that the purpose of this outer-layer damping is to reduce the computational time step, which is limited by the  $CFL$  number,  $CFL = \max_{1 \leq i \leq 3} (|u_i| \Delta t / \Delta x_i)$ . Here  $|u_i|$  is the maximum instantaneous velocity in the  $i$ th direction and  $\Delta x_i$  is the corresponding grid spacing at that location. Note that the viscous  $CFL$  number does not become significant in any of the simulations performed here. For minimal-span channels at  $Re_\tau = 590$  with no outer-layer damping, the maximum  $CFL$  number occurs in the outer layer due to the large streamwise velocity. We see the time step improves by roughly 20–24% with the use of the outer-layer damping (table 1, set

$S_{3a}$ ) than without (set  $S_2$ ). This means the simulations can be completed quicker and hence use less computational resources. However, at higher friction Reynolds numbers of  $Re_\tau = 2000$  (set  $S_{3c}$ ), the time step for the smooth wall with outer-layer damping is unaltered compared to the case without (set  $S_2$ ). This is due to the use of the cosine mapping to define the wall-normal grid, which produces a very fine grid near the wall especially for high Reynolds number cases. As a result of such a small  $\Delta z$ , the wall-normal  $CFL$  number is now maximum and this occurs in the near-wall region, which is independent of the outer-layer damping. If a more appropriate mapping was used for these high friction Reynolds numbers, we would expect a similar improvement in time step as at  $Re_\tau = 590$ .

The most appropriate position for  $z_d$  is difficult to establish from the above data. A minimum of  $z_d^+ \approx 200$  seems necessary to ensure that the damping does not interact with the near-wall flow. It also seems reasonable that  $z_d$  should scale in some way on  $z_c$ , for larger domain widths. The three sets of simulations suggest that  $z_d$  should be roughly two times  $z_c$ , so a tentative rule of thumb would be  $z_d^+ \gtrsim \max(200, 2z_c^+)$ . For an appropriate wall-normal mapping, this allows a 20–24% improvement in the computational time step.

### 3.3. Streamwise domain length (sets $S_{4a}$ and $S_{4b}$ )

In the previous simulations, the streamwise length was fixed at  $L_x/h = 2\pi$ , which corresponds to a viscous length of about  $3700\nu/U_\tau$  at  $Re_\tau = 590$ . This is regarded as being a suitable length for full-span simulations at this friction Reynolds number [32]. However, this length is only necessary due to the large outer-layer structures which are present in the full-span simulations, which have streamwise lengths on the order of the channel half-height,  $h$ . The minimal-span channel only captures the inner flow, so it is likely a shorter length can be used.

The near-wall cycle of the buffer layer produces streaky structures with streamwise lengths of 1000 viscous units [33]. However, these low- and high-speed streaks are nearly two-dimensional, which suggests they could be represented in the infinite ( $k_x = 0$ ) mode and hence the domain length doesn't have to be this long. These streaks are accompanied by quasi-streamwise vortices [34], which extend into the logarithmic layer. These have streamwise lengths which scale as roughly 2–3 times their spanwise width [3, 7]. The minimum spanwise domain width that can sustain turbulence is around 100 viscous units [1], which means the smallest vortices that need to be captured would have a streamwise length of 200–300 viscous units. Simulations with larger spanwise domain widths would produce vortices with longer streamwise lengths, so that the largest captured eddy would have spanwise and streamwise lengths of  $\lambda_y = L_y$  and  $\lambda_x = 2-3L_y$ .

Two different spanwise domain widths are investigated for varying the streamwise length (table 1, set  $S_4$ ). Firstly, the smallest width of  $L_y^+ \approx 120$  (set  $S_{4a}$ ) would have the largest eddies having streamwise lengths of  $\lambda_x^+ = 240-350$ . Various streamwise domain lengths of  $L_x^+ = (190, 300, 460, 930, 1850)$  are chosen to see how this affects the largest eddies. The second spanwise domain width of  $L_y^+ \approx 350$  (set  $S_{4b}$ ) would be able to capture larger eddies, the largest of which would have a streamwise length of roughly  $\lambda_x^+ = 710-1100$ . The same set of streamwise domain lengths are simulated for this wider domain. A standard-height channel is used, with no outer-layer damping,  $K_i = 0$ .

Figure 6 shows the mean velocity profile for the two spanwise widths, for all the streamwise lengths tested. For the smaller domain width (figure 6a,b), the shortest streamwise lengths of  $L_x^+ \approx 190$  and 300 result in a reduction in the smooth-wall velocity above  $z^+ \gtrsim 20$ . There is also a slight increase in the centreline velocity. As a result, the difference in smooth- and rough-wall velocity (inset of figure 6b) decreases relative to the full-span and longer minimal-span cases. Note that while the grid resolution is different for these shorter channels (set  $S_{4a}$ , table 1) which may explain this effect, it will later be seen in the wider channels that have the same grid resolution differences (set  $S_{4b}$ ) that this is not the case. Little discernible difference can be seen between the longer streamwise lengths of  $L_x^+ \geq 460$ , in agreement with the scalings

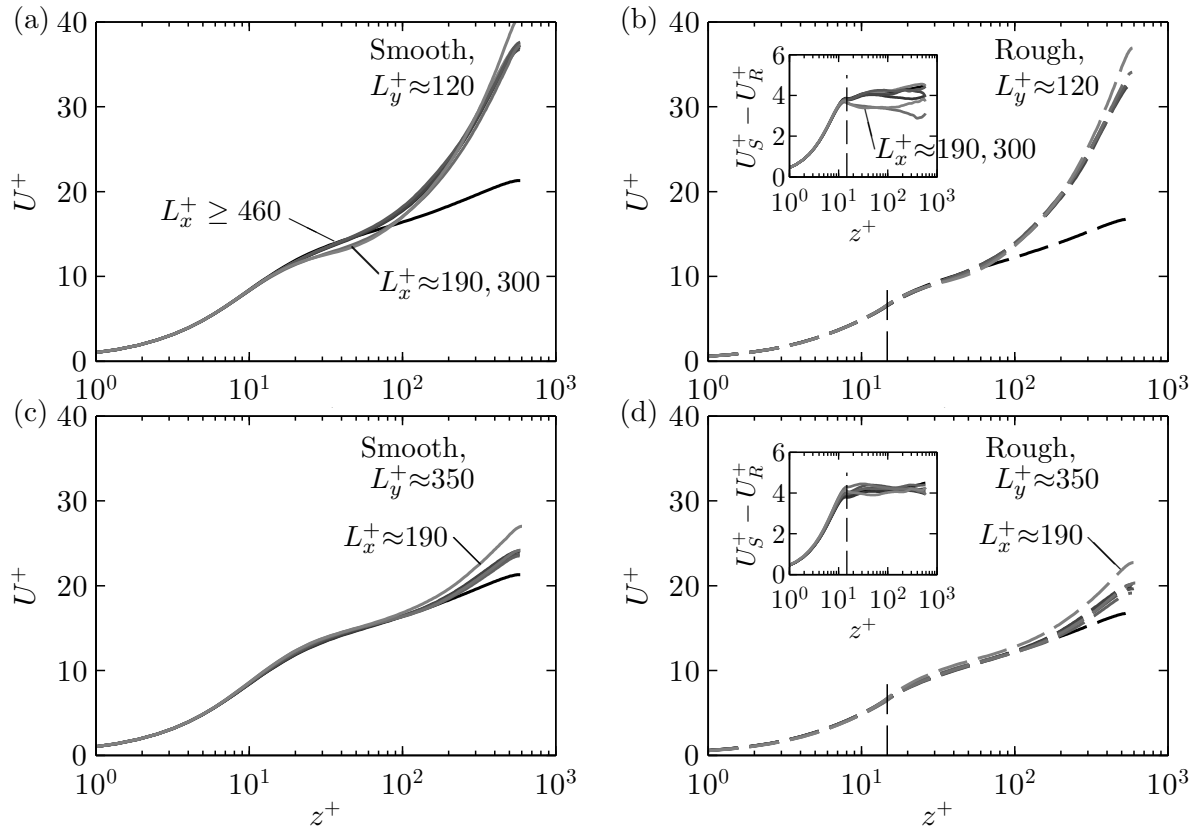


Figure 6: Streamwise velocity profile for varying streamwise length for (a,c) smooth- and (b,d) rough-wall standard-height channels. Spanwise domain width is (a,c)  $L_y^+ \approx 120$  (set  $S_{4a}$ ) and (b,d)  $L_y^+ \approx 350$  (set  $S_{4b}$ ). Line styles are: black, full-span channel; grey, minimal-span channel with varying streamwise length (dark grey is longer), refer table 1; Vertical dashed line indicates the roughness height  $k = h/40$ . Insets of (b,d) shows difference in smooth and rough wall flows.

discussed above. This also indicates that the low- and high-speed streaks, with lengths of 1000 viscous units, do not need to be explicitly captured. The case of  $L_x^+ \approx 300 = 2.5L_y^+$  produces an incorrect profile and this suggests that a minimum streamwise length of  $L_x^+ = 3L_y^+$  is required, especially for narrow channels in which  $z_c$  is closer to the buffer layer than log layer of the flow.

The smallest streamwise length of  $L_x^+ \approx 190$  was unable to sustain turbulence for a prolonged period. It would decay to a laminar state after  $T^+ = tU_\tau^2/\nu \approx 14.8 \times 10^4$  in the smooth-wall channel, and after  $T^+ \approx 9.7 \times 10^4$  in the rough-wall channel. The data shown in the previous figures for this streamwise length is averaged only when the flow is turbulent. This behaviour is similar to what was observed in [1], who showed that turbulence could not be maintained in channels with streamwise lengths of around 200 viscous units. As discussed above, this is because it is shorter than the quasi-streamwise vortices which have streamwise lengths of  $\lambda_x^+ \approx 200-300$ .

The larger spanwise domain (figure 6c,d) shows that the shortest streamwise length of  $L_x^+ = 190$  restricts the size of the eddies so that the spanwise size of the largest eddy is smaller than the spanwise width of the domain. The resulting velocity profile more closely resembles that of the narrower spanwise width seen in figure 6(a,b). Interestingly, the streamwise length of  $L_x^+ \approx 300$  appears to agree quite well with the cases with longer lengths. This is in contrast to the narrow domain (figure 6a), which shows a clear difference for  $L_x^+ \approx 300$ . Even the case with  $L_x^+ \approx 460 = 1.3L_y^+$  is producing a velocity profile and roughness function comparable to that of

channels with longer streamwise lengths, despite not having the requisite scaling of  $L_x^+ \gtrsim 2-3L_y^+$  discussed above. This is similar to the results of [35] who looked at wide spanwise channels with very short streamwise lengths. The velocity profiles they obtained look similar to a full-span full-length channel, and there is no apparent increase in streamwise velocity in the outer layer that is characteristic of minimal-span channels. A possible explanation for the results seen here is that the wall-normal critical location  $z_c^+ \approx 140 = 0.24h^+$  is outside the log-layer, which is generally believed to end at  $z \approx 0.15h$  [36]. As such, the expected streamwise length scale of  $2-3L_y$  is no longer appropriate in the outer layer. In this case, the largest eddy at the edge of the logarithmic layer would have a streamwise length of roughly  $\lambda_x^+ \approx 440-660$ , potentially explaining why the simulation with  $L_x^+ \approx 460$  still produces a reasonable velocity profile.

Given the above results, it is possible to restrict the streamwise length to  $L_x = 3L_y$ . However, for very narrow channels this can result in a streamwise domain length less than 1000 viscous units. While it appears the buffer-layer streaks do not need to be captured in the domain, having such a small streamwise domain exasperates the bursty nature of the minimal-span channel [17]. Only one or maybe two quasi-streamwise vortices are present in the domain, which makes obtaining converged statistics difficult as the simulation needs to be run for a significantly long time. We believe that a minimum streamwise length of roughly 1000 viscous units seems a reasonable length in these cases, so that several quasi-streamwise vortices are present. As with the spanwise domain width recommendations in [5], the streamwise length should be larger than the characteristic streamwise length scale of the roughness,  $\lambda_{r,x}$ , if it were present. As such, we have  $L_x \gtrsim \max(3L_y, 1000\nu/U_\tau, \lambda_{r,x})$ .

### 3.4. Temporal Sweep (set $S_5$ )

In this section, the temporal sweep (§2.1) is performed in a standard-height channel, with no outer-layer damping ( $K_i = 0$ ) and a streamwise length of  $L_x/h = 2\pi$ , corresponding to  $L_x^+ \approx 3700$  at the start of the sweep (table 1). The roughness height is fixed at  $k = h/40$ , so the roughness Reynolds number varies as  $15 \lesssim k^+ \lesssim 50$ . Three different sweeps were conducted in which the pressure gradient parameter at the end of the sweep is  $\Delta_{p,Re_\tau=180} = (0.03, 0.07, 0.15)$ .

Figure 7 shows the mean velocity profiles for the fastest and slowest sweeps, comparing the sweep data with full-span steady-flow data at the highest and lowest friction Reynolds numbers tested. Figure 7(a,b) shows the mean velocity for the slowest sweep, when the pressure gradient parameter (6) at  $Re_\tau \approx 180$  was  $\Delta_{p,Re_\tau=180} = 0.03$ . Figure 7(c,d) shows the mean velocity for the fastest sweep, with  $\Delta_{p,Re_\tau=180} = 0.15$ . To obtain statistics for a desired  $Re_\tau$ , time-averaging is performed over a window of  $\pm 10\%$  of that value. At the initial friction Reynolds number of the simulation,  $Re_\tau = 590$ , both the sweeps (figure 7a,c) show good agreement with the full-span channel in the near-wall region. As the spanwise width is  $L_y/h = 0.6$ , then the critical wall-normal location is approximately  $z_c^+ \approx 0.4L_y^+ = 142$  which agrees well with the figure. As  $\Delta_p$  is not significant yet (figure 2b) then there is little difference between the two sweeps.

However, at the end of the sweep when the friction Reynolds number is close to  $Re_\tau = 180$  and the  $\Delta_p$  is maximum, then differences start to emerge. The slowest sweep (figure 7b) has reasonable agreement very close to the wall below  $z^+ \lesssim 15$ , but the pressure gradient has reduced the streamwise velocity compared to the full-span steady flow. Importantly though is that the difference between the smooth and rough-wall flows (inset of figure 7b) agrees quite well with the full-span data. Taking the difference between two flows with the same weak pressure gradient ostensibly still produces a correct estimate of  $\Delta U^+$ . However, when the pressure gradient is increased to  $\Delta_{p,Re_\tau=180} = 0.15$  (figure 7d) then larger differences are seen. The near-wall region has been noticeably changed, and the difference in smooth and rough wall velocity (inset) is seen to overestimate the full-span data. Note that the data have been ensemble averaged over four runs, so that the amount of time the flow is averaged over is the same as in the slowest sweep. This therefore indicates that the overestimation of  $\Delta U^+$  is a direct result of the stronger

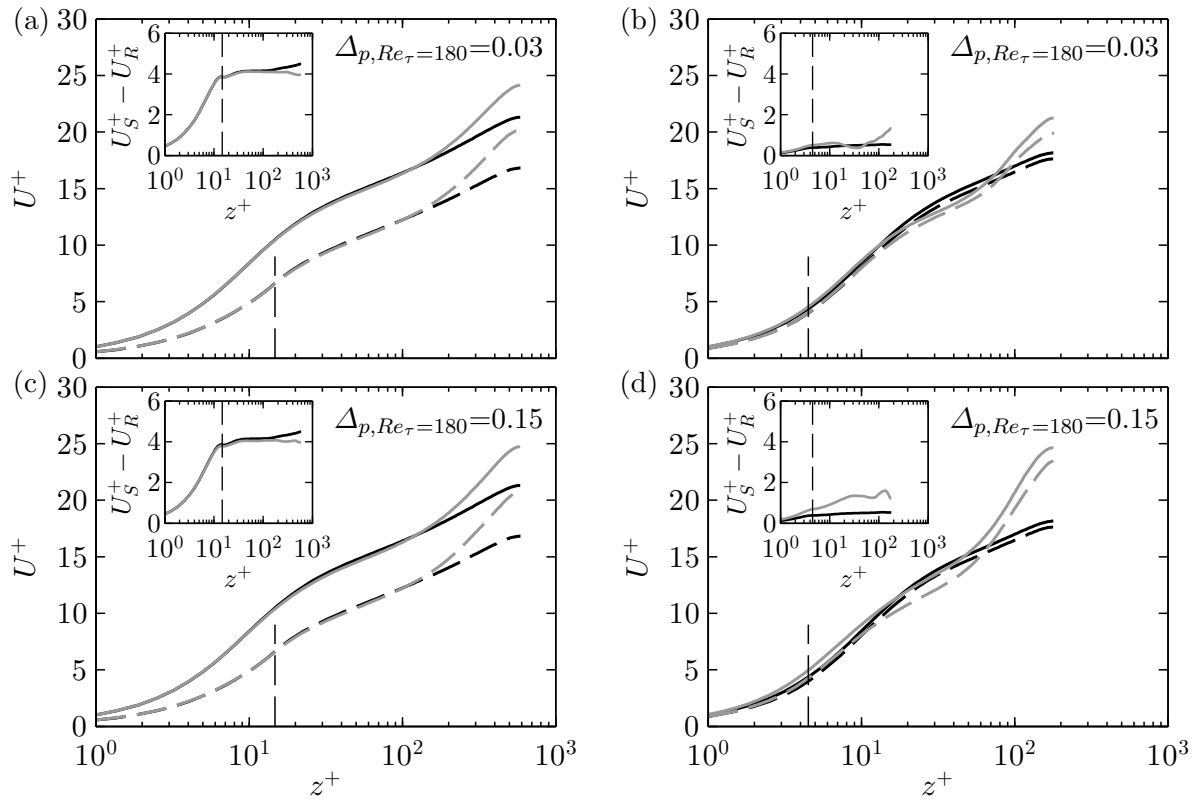


Figure 7: Mean streamwise velocity profile for (a,c)  $Re_\tau \approx 590$  and (b,d)  $Re_\tau \approx 180$ , from full-span steady flow (black line) and temporal sweep (grey line). (a,b) slowest sweep ( $\Delta_{p, Re_\tau=180} = 0.03$ ) and (c,d) fastest sweep ( $\Delta_{p, Re_\tau=180} = 0.15$ ), §2.1. Line styles: Solid line, smooth wall; dashed line, rough wall; vertical dashed line, roughness crest,  $k = h/40$ . Inset shows difference in smooth- and rough-wall velocity.

pressure gradient.

The roughness function  $\Delta U^+$  is now computed from the difference in smooth and rough-wall flows at matched  $U_\tau$  values. As seen in the insets of figure 7, the smooth- and rough-wall velocity difference is not constant with  $z^+$  as in the steady data. This indicates that the flow has not been averaged for long enough at the desired  $Re_\tau$  value. As such, multiple sweeps from different initial conditions would need to be conducted to obtain a converged outer region. However, for the purposes of this investigatory study, the velocity difference is averaged from the crest of the roughness to the channel centre to obtain an estimate of  $\Delta U^+$ . This is done for a range of friction Reynolds numbers, with the resulting data plotted in figure 8 against the equivalent sandgrain roughness,  $k_s^+$ . Ideally, the temporal sweep data (lines) should agree with the steady flow data (black symbols). Indeed, the temporal sweep does show promise in this regard, especially for the weaker pressure gradient cases (slower sweeps). It is especially good considering the level of error that is normally associated with experimental studies (grey circles).

It appears as though the sweep approach to determining the hydraulic behaviour of roughness could work, although only for the slowest sweep tested. Hence, a pressure gradient parameter of  $\Delta_p \leq 0.03$  is required, which is close to the recommendation in [25] that zero pressure gradient conditions can be assumed when  $\Delta_p \leq 0.01$ . A value of  $\Delta_p \geq 0.07$  results in pressure gradient effects that lead to inaccuracies in  $\Delta U^+$ . Future studies could prescribe a constant value of  $\Delta_p$  rather than linearly varying the bulk velocity, as this would ensure pressure gradient effects

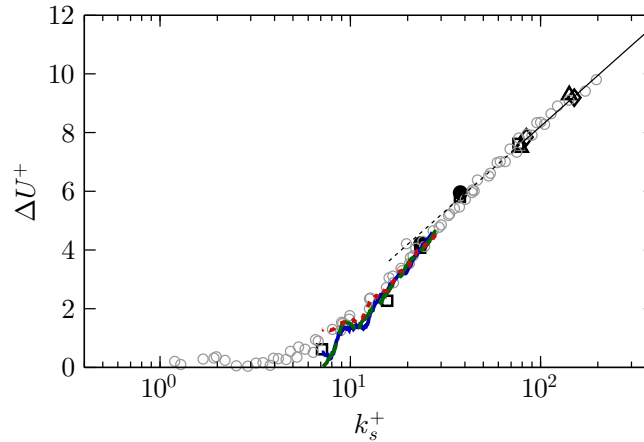


Figure 8: Hama roughness function for the temporal sweep with modelled roughness at fixed  $k = h/40$ , where  $k_s^+ \approx 1.6k^+$ . Symbols: grey circles, uniform sand grains of Nikuradse (1933) [37]; black symbols, steady flow data for the same modelled roughness [5]; blue solid line, sweep data for  $\Delta_{p, Re_\tau=180} = 0.03$  (slowest sweep); green dashed line, sweep data for  $\Delta_{p, Re_\tau=180} = 0.07$ ; red dotted line, sweep data for  $\Delta_{p, Re_\tau=180} = 0.15$  (fastest sweep).

remain negligible, while efficiently traversing the range of roughness Reynolds numbers.

#### 4. Conclusions

In this paper, a series of improvements to the minimal-span channel were investigated. The goal is to obtain a direct measure of  $\Delta U^+$  by only capturing the relevant near-wall scales. Three improvements are suggested. First, a half-height channel was used in which a slip-wall is positioned at the channel centre. This allows for the number of grid points to be halved, at the cost of running the simulation for twice as long to reach the same level of statistical convergence. It is up to the user to balance this trade off between memory and time. Second, a forcing was applied to the outer layer to reduce the centreline velocity. This allowed for an improvement in the time step of around 20–24%, although this did not extend to higher friction Reynolds numbers due to the grid using a cosine mapping in the wall-normal direction. The present data suggest that the location at which the forcing starts should be  $z_d^+ \gtrsim \max(200, 2z_c^+)$ . The first constraint is present for very narrow channels where  $z_c^+$  is close to the wall, as the forcing will interfere with the near-wall flow otherwise. Third, the streamwise length was investigated, independent of the previous two improvements. It appears that the length should be long enough to capture the largest log-layer eddy which implies  $L_x = 3L_y$ , where  $L_y \gtrsim \max(100\nu/U_\tau, k/0.4, \lambda_{r,y})$  is obtained from the guidelines in [5],  $\lambda_{r,y}$  being some characteristic spanwise length scale. However, for very narrow channels the bursty nature of the minimal-span channel and small spatial domain makes obtaining converged statistics a very time-consuming process, so a minimum length of 1000 viscous units is necessary. As such, the recommendation for the streamwise domain length is  $L_x \gtrsim \max(3L_y, 1000\nu/U_\tau, \lambda_{r,x})$ , where  $\lambda_{r,x}$  is the characteristic streamwise length scale of the roughness. Finally, a temporal sweep was conducted to see if the full roughness behaviour could be obtained by varying the roughness Reynolds number. A simple linear variation in the bulk velocity was tried, with three different rates of change investigated. This was independent of the previous improvements. It was shown that the slowest rate of change, with a final pressure gradient parameter value of  $\Delta_{p, Re_\tau=180} = 0.03$  could reasonably predict some of the  $\Delta U^+$  vs  $k_s^+$  curve. Larger values of  $\Delta_p$  resulted in substantial flow changes compared to the steady flow and so are not feasible.

It is important to consider the cost of the minimal-span channel relative to the full-span

channel. Both the memory and computational time need to be analysed, where the former can be easily described by the grid size while the latter is more involved. In standard DNS full-span channel studies, at least 10 large-eddy turnover times are recommended to obtain converged first- and second-order statistics (see for example [31]). For a full-span channel this corresponds to  $T = 10U_\tau/h$ . However, if we only want to converge statistics up to the height  $z = z_c < h$ , then we only need 10 eddy turnovers of this  $z_c$ -sized eddy and so  $T_{z_c} = 10U_\tau/z_c$ . This argument assumes a fairly large spatial domain so that there are actually a large number of  $z_c$ -sized eddies present in the full-span channel at any instant. In a minimal-span channel, only a few such eddies could be present in the small domain at any instant. We would therefore need to run the simulation for long enough to observe the same number of  $z_c$ -sized eddies as would be seen in the full-span channel, presumably resulting in the same level of convergence. This costing argument together with user-decided trade-offs is to be detailed in a future paper.

### Acknowledgments

Computational time was granted under the Victoria Life Sciences Computational Initiative, which is supported by the Victorian Government, Australia. The authors would also like to acknowledge the funding provided to the Multiflow program by the European Research Council.

### References

- [1] Jiménez J and Moin P 1991 *J. Fluid Mech.* **225** 213–240
- [2] Hamilton J M, Kim J and Waleffe F 1995 *J. Fluid Mech.* **287** 317–348
- [3] Flores O and Jiménez J 2010 *Phys. Fluids* **22** 071704
- [4] Hwang Y 2013 *J. Fluid Mech.* **723** 264–288
- [5] Chung D, Chan L, MacDonald M, Hutchins N and Ooi A 2015 *J. Fluid Mech.* **773** 418–431
- [6] Jiménez J and Pinelli A 1999 *J. Fluid Mech.* **389** 335–359
- [7] Hwang Y 2015 *J. Fluid Mech.* **767** 254–289
- [8] Hama F R 1954 *Trans. Soc. Naval Arch. Mar. Engrs* **62** 333–358
- [9] Flack K A, Schultz M P and Shapiro T A 2005 *Phys. Fluids* **17** 035102
- [10] Townsend A A 1976 *The Structure of Turbulent Shear Flow* 2nd ed (Cambridge University Press)
- [11] Efros V and Krogstad P Å 2011 *Exp. Fluids* **51** 1563–1575
- [12] Chan L, MacDonald M, Chung D, Hutchins N and Ooi A 2015 *J. Fluid Mech.* **771** 743–777
- [13] Flores O and Jiménez J 2006 *J. Fluid Mech.* **566** 357–376
- [14] Mizuno Y and Jiménez J 2013 *J. Fluid Mech.* **723** 429–455
- [15] Chung D, Monty J P and Ooi A 2014 *J. Fluid Mech.* **742** R3
- [16] Jiménez J, Kawahara G, Simens M P, Nagata M and Shiba M 2005 *Phys. Fluids* **17** 015105
- [17] Jiménez J 2015 *Phys. Fluids* **27** 065102
- [18] Spalart P R, Moser R D and Rogers M M 1991 *J. Comput. Phys.* **96** 297–324
- [19] Kim J and Moin P 1985 *J. Comput. Phys.* **59** 308–323
- [20] Lundbladh A, Berlin S, Skote M, Hildings C, Choi J, Kim J and Henningson D S 1999 An efficient spectral method for simulation of incompressible flow over a flat plate *TRITA-MEK* 1999/11 KTH, Stockholm
- [21] Bernardini M, Pirozzoli S, Quadrio M and Orlandi P 2013 *J. Comput. Phys.* **232** 1–6
- [22] Busse A and Sandham N D 2012 *J. Fluid Mech.* **712** 169–202
- [23] Borrell G 2015 *Entrainment effects in turbulent boundary layers* Ph.D. thesis Technical University of Madrid
- [24] Jiménez J 2004 *Annu. Rev. Fluid Mech.* **36** 173–196
- [25] Patel V 1965 *J. Fluid Mech.* **23** 185–208
- [26] Jones M, Marusic I and Perry A 2001 *J. Fluid Mech.* **428** 1–27
- [27] Seddighi M, He S, Vardy A and Orlandi P 2014 *Flow Turbul. Combust.* **92** 473–502
- [28] Lam K and Banerjee S 1992 *Phys. Fluids* **4** 306–320
- [29] Handler R A, Saylor J R, Leighton R I and Rovelstad A L 1999 *Phys. Fluids* **11** 2607–2625
- [30] Nagaosa R 1999 *Phys. Fluids* **11** 1581–1595
- [31] Hoyas S and Jiménez J 2006 *Phys. Fluids* **18** 011702
- [32] Chin C, Ooi A S H, Marusic I and Blackburn H 2010 *Phys. Fluids* **22** 115107
- [33] Kline S J, Reynolds W C, Schraub F A and Runstadler P W 1967 *J. Fluid Mech.* **30** 741–773
- [34] Jeong J, Hussain F, Schoppa W and Kim J 1997 *J. Fluid Mech.* **332** 185–214
- [35] Toh S and Itano T 2005 *J. Fluid Mech.* **524** 249–262
- [36] Marusic I, Monty J P, Hultmark M and Smits A J 2013 *J. Fluid Mech.* **716** R3
- [37] Nikuradse J 1933 Laws of flow in rough pipes. English translation published 1950, NACA Tech. Mem. 1292